Review Article **Open Access**

Simon Peter Mekhail, Gordon Arbuthnott, and Síle Nic Chormaic*

Advances in Fibre Microendoscopy for Neuronal Imaging

DOI 10.1515/odps-2016-0003
Received July 14, 2016; revised October 29, 2016; accepted October 31, 2016

Abstract: Traditionally, models for neural dynamics in the brain have been formed through research conducted on slices, with electrodes, or by lesions to functional areas. Recent developments in functional dyes and optogenetics has made brain research more accessible through the use of light. However, this improved accessibility does not necessarily apply to deep regions of the brain which are surrounded by scattering tissue. In this article we give an overview of some of the latest methods in development for neural measurement and imaging. We specifically address methods designed to overcome the problem of imaging *in-vivo* for regions far beyond the mean free path of photons in brain tissue. These methods would permit previously restricted neural research.

Keywords: in-vivo; scattering media; image reconstruction; phase correction

1 Introduction

To motivate the use of light in neuroscience, consider the striatum of a mouse, a 1.5 mm wide nucleus among the basal ganglia. It has been known for its role in the coordination of motor control, neural reward and punishment, and learning since the 1800s [1, 2]. Disorders, such as Parkinson's disease, motivated much research into the function of this nucleus over the last two centuries. Early research, however, was conducted by lesioning the striatum and produced conflicting results; some reported uninhibited movement in which an animal would run uncontrollably [3], while others reported that the lesions had little effect or even reduced movement [4]. In the 1980's a new model grounded on anatomy and clinical speculation suggested the existence of two output pathways from the striatum; one for stimulating desired movement and another inhibiting undesired movement [5]. These pathways, named the direct and indirect pathways respectively, are difficult to observe separately for two reasons: (i) they exist at the same place within the striatum making the neurons difficult to physically separate [6] and (ii) the electrophysiological characteristics are indistinguishable, thereby making electrode measurements ambiguous [5]. The pathways can, however, be distinguished genetically. Direct pathway neurons (D1 neurons) and indirect pathway neurons (D2 neurons) express the dopamine receptors Drd1 and Drd2, respectively. Due to the opposing effects of these receptors, they exist almost exclusively in their own pathway with only $\sim$5% of striatal neurons expressing both [5]. Specific targeting of these pathways can, therefore, be achieved by engineering a virus with the genetic code of a desired indicator protein such that it will only infect cells expressing the gene for either Drd1 or Drd2. GCaMP, a protein fluorescing green in the presence of calcium, thereby indicating cell activity, was first used to virally target specific cells of mice in 2004 [7]. The following year, a similar method was used with Channelrhodopsin-2 (ChR2)- a cation channel which allows for light-mediated neural stimulation - in transgenic mice [8]. Hence, an all-optical means for directly stimulating and monitoring neural activity in targeted cells is now possible. The problem which remains is that of bringing light to the target areas in a manner suitable for stimulation and imaging.

***Corresponding Author: Sıle Nic Chormaic:** Light-Matter Interactions Unit, Okinawa Institute of Science and Technology Graduate University, Onna, Okinawa 904-0495, Japan, E-mail: sile.nicchormaic@oist.jp
Simon Peter Mekhail: Light-Matter Interactions Unit, Okinawa Institute of Science and Technology Graduate University, Onna, Okinawa 904-0495, Japan
Gordon Arbuthnott: Brain Mechanisms for Behaviour Unit, Okinawa Institute of Science and Technology Graduate University, Onna, Okinawa 904-0495, Japan

2 Challenges in Traditional Microscopy

The greatest hindrance to effective deep tissue imaging is light scattering. The distance travelled by a non-

interacting (ballistic) photon can be explained by Beer-Lambert exponential decay [9]

$$P(z) = e^{-\mu_s z}, \quad (1)$$

where z is the distance along the optical axis and $P(z)$ is the proportion of incident photons which are ballistic at z. The mean free path (MFP) is the reciprocal of the scattering coefficient, μ_s. Anisotropic Mie scattering[1] caused by cellular organelles dominates in biological tissue [10]. Scattering heavily favours the forward direction and the anisotropy can be quantified by a dimensionless parameter, g. A typical value for g in tissues is 0.9 [9, 11–13]. The reduced scattering coefficient, μ_s', takes this large anisotropy into account and is defined as $\mu_s' = \mu_s(1-g)$. The transport mean free path (TMFP), defined as $1/\mu_s'$, is the average distance a photon can travel into a material while maintaining some correlation to its original trajectory [14]. Beyond this length the majority of photons can be considered to be diffuse. Figure 1 shows such anisotropic scattering in tissue along the optical axis. Jacques [13] summarised data collected from 56 sources to estimate μ_s' in biological tissue using a model for wavelength-dependent Mie scattering such that

$$\mu_s' = a\left(\frac{\lambda}{500\text{nm}}\right)^{-b}, \quad (2)$$

where λ is the vacuum wavelength in nanometres. For brain tissue, the constants a and b are 24.2 cm^{-1} and 1.611, respectively. The model is valid for wavelengths in the range 400-1300 nm.

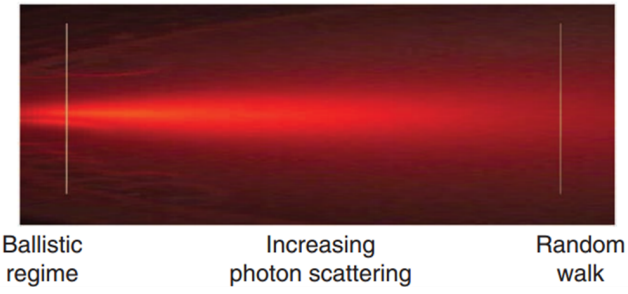

Figure 1: Light propagation through a scattering tissue. Boarders showing the MFP (left) and the TMFP (right) for $g = 0.9$. Reprinted by permission from Macmillan Publishers Ltd: Nature Methods [11], copyright (2010).

In an ideal imaging system all excitation photons would be ballistic which would limit most imaging to depths within one MFP. For 488 nm, the excitation wavelength for GCaMP, Equation 2 gives an estimated MFP of 40 µm with some indication that this value diminishes with the age of the animal used [15]. Large anisotropy means that the distortion to the point spread function (PSF) would not be significant just beyond the MFP; hence, with deconvolution, or if some resolution loss can be tolerated, epifluorescence microscopy could extend as far as 50-100 µm into brain tissue [16, 17]. Confocal microscopy allows for an increase in depth without significant loss of resolution as the scattered photons are rejected by an imaging pinhole. Since only ballistic photons contribute to the image, the signal decreases exponentially with penetration depth in accordance with Equation 1. This can be remedied by increasing the input power with depth. For cellular resolution, the depth can be extended to approximately 250 µm before multiple scattering events render the pinhole ineffective [11].

A more subtle problem that must be considered when using this technique is the amount of light incident on the sample. For live cell imaging, the illumination power must be limited to prevent cell damage [18]. Most photons in deep confocal microscopy are completely rejected meaning that large illumination powers are required. For an anisotropy parameter of 0.9 at half the TMFP only 0.7% of photons are ballistic and, therefore, contribute to the image. Reports suggest that a localised high intensity, rather than a high total photon dose, is the cause of cellular damage [19–21]. Light sheet microscopy accounts for this by using a cylindrical lens to illuminate a single plane at the object. Illumination is aligned perpendicularly to the imaging axis. This method allows for fast acquisition, as it is scanner free, and optical sectioning, since only the imaging plane is illuminated. Light sheet phototoxicity is so low that it is reported to be effective at imaging live cells during anaphase of mitosis, a highly light-sensitive period of the cell life cycle [19]. The cumbersomeness of requiring perpendicular objectives for this technique was mitigated by Bouchard *et al.* [22] who describe a method in which a single objective is used for both excitation and imaging of *in-vivo* brain tissue, see Figure 2. This method, known as swept confocally-aligned planar excitation (SCAPE) microscopy, fulfils many requirements for *in-vivo* imaging, yet the maximum depth possible is no greater than traditional confocal microscopy, with Bouchard *et al.* reporting a depth of 140 µm [22].

Two-photon fluorescence (2P) is currently the leading technique for deep, non-invasive imaging. It requires the use of lower energy wavelengths since it depends on the simultaneous (within ~1 fs) absorption of more than one photon by a fluorophore. As this is very unlikely, the exci-

1 Mie regime: scattering particles are the same order of magnitude as the wavelength, λ.

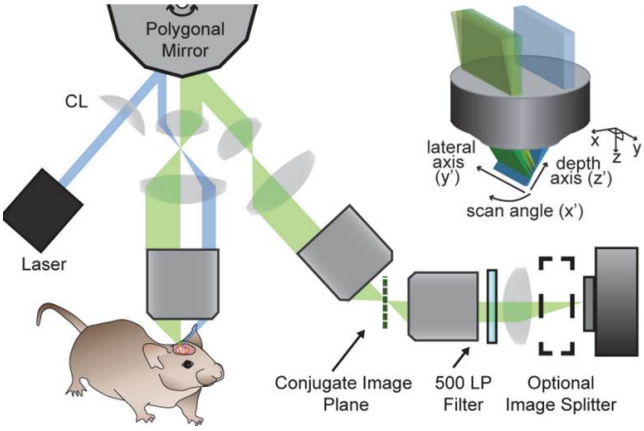

Figure 2: *In-vivo* SCAPE microscopy set up; CL, cylindrical lens. Reprinted by permission from the Optical Society of America: Optics in Life Sciences [23], copyright(2015).

tation must be focussed tightly in space as well as in time with transform limited pulses. The typical enhancement achieved in 2P fluorescence by using a pulsed laser instead of a continuous wave laser is around 10^5 [9]. This method has a similar PSF to that for confocal microscopy, which is the square of the epifluorescence PSF and, as in the confocal system, only ballistic photons contribute to the signal. The nonlinear absorption makes out-of-focus fluorescence very improbable. Furthermore, the low absorption of near infra-red (NIR) light in tissue significantly reduces phototoxicity. Yet limitations exist. The emitted photons have visible wavelengths and, for typical 2P imaging depths, undergo multiple scattering events on their path to the detector. At the surface of the tissue these photons are diffuse and have a broad intensity distribution with a full-width-at-half-maximum (FWHM) 3/2 times the imaging depth regardless of the MFP [9]. As the depth increases, a larger portion of fluorescence falls outside the reach of the collection optics. Increasing power to combat scattering at depth eventually leads to surface and out-of-focus fluorescence. Furthermore, the increased depth reduces the numerical aperture (NA) rapidly since the outer regions of the focussing cone of light scatter more [24]. For imaging cells, the largest reported depths in the brain are around 1 mm [25–27]. This technique greatly facilitated *in-vivo* cortical research in both behaving and anaesthetized animals with surgically-mounted skull windows [9, 28, 29, 29, 30]. This method, however, does not reach the basal ganglia and, for this reason, we turn our attention to implanted devices.

3 Constraints on Problem

The methods discussed above outline the motivations behind- and short comings of- using light for deep-brain research. While strides have been made in deeper non-invasive imaging, the need for an implanted device remains clear. Although the implanted technologies discussed in the following sections are not specifically designed for imaging the striatum, we discuss them with reference to the problem outlined in the Introduction. We do this as the chosen problem presents us with a rather complete set of criteria against which an imaging technique can be critiqued. The depth, ∼3 mm, is beyond any imaging modality available. The required resolution is sub-cellular for the identification of specific cell types and structures. For calcium transients to be distinguishable, a temporal resolution of ∼10 Hz is required. For live cells, the intensity delivered to the tissue must be in the range of 10 Wcm^{-2} [19]. Gliosis expected around the tip of the implant requires a working distance greater than 5 µm [31] and, hence, a method for selecting a focal plane. The size of the implant must be small to minimise damage. Cortical blood vessels could have spacings as small as 200 µm [32]. Some sources claim probes larger than ∼300 µm could have detrimental effects on the mice [33]. Finally, since we are observing a nucleus largely responsible for coordinating movement, a flexible probe is preferred.

4 Fibre Probes and Endoscopes

4.1 Electrodes and Photometry

Although we primarily discuss the exclusive use of optics in monitoring and stimulating neural activity, electrophysiological methods have been used in monitoring cells which can only be separated genetically. Kravitz and Kreitzer [35] described a procedure in which electrodes monitored the electrical activity of a few D1 and D2 neurons. The neurons in a specific pathway were targeted with ChR2 making them excitable under 480 nm light. The recordings made by the electrodes while the light was off could be correlated to those made during optical stimulation, giving some idea of whether the cell being recorded was D1 or D2. The combined optical fibre and electrodes system had a total cross-sectional diameter of just over 125 µm. This method, though clever and minimally invasive, lacks spatial information of the cells and cannot be performed with passive observation. The viral targeting and monitoring of specific neural cells in mice has since been ex-

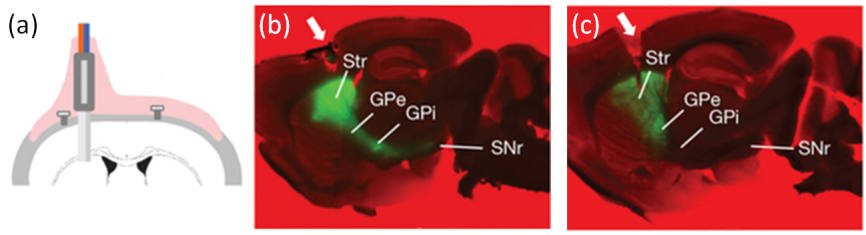

Figure 3: Striatum photometry; (a)illustration of implanted excitation(blue) and emission(red) fibres, (b) and (c) bright field and fluorescence image of slices for (b) direct-pathway- and (c) indirect-pathway-labelled transgenic mice. White arrows show the implant locations. Adapted by permission from Macmillan Publishers Ltd: Nature [34], copyright (2013)

tended to a purely optical endeavour. Chronic multimode fibre implants collect fluorescence from calcium indicators, such as GCaMP, which are expressed in the targeted cells as shown in Figure 3. The mice are free to move while the cell activity is recorded, thereby allowing for the correlation of activity in a given pathway with the actions of the mice [34, 36, 37]. Implanted fibres have also been used in stimulating ChR2-expressing neurons causing a notable change in the behaviour of the animal [37]. The benefit of the purely optical probes over electrodes is that they allow for direct passive measurement of many cells of a specific pathway or type. This is done at the expense of some spatial information and temporal resolution offered by electrode arrays. The method has also been extended to measure the spectrum as well as the intensity from the collection fibre. It was shown in 2014 that it could be used in Förster resonance energy transfer (FRET) microscopy [38].

4.2 Implanted Lenses

The above methods present alternatives to imaging in order to satisfy the size constraints, yet developments in endoscopy over the past decade have all but met these tight constraints for *in-vivo* imaging. Traditionally, rigid Hopkins endoscopes comprising of a series of microlenses arranged in a thin tube were used. These were shown to be effective in confocal and structured illumination endoscopy [39], but the rigid body and large diameters of 1-3 mm made them unsuitable for *in-vivo* brain imaging. Graded index (GRIN) lenses somewhat remedied the size problem. Rather than refracting light through a curved surface, rod-shaped, GRIN lenses have a radially varying refractive index. Used as chronic implants, these lenses would enable optical access to deep brain structures, but would initially require that the animals remain stationary. The GRIN setups were shown to be effective with fast wide-field, high resolution two-photon fluorescence, and super resolution single photon microscopy [15, 40–43]. To allow for movement of the animal, in recent years miniaturised, head-mounted microscopes, as shown in Figure 4, have been developed. Betley *et al.* reported on the use of a 0.5 mm GRIN lens with a head-mounted microscope for deep brain fluorescence imaging in the arcuate nucleus (ARC) [44]. To do this, a 0.6 mm diameter cylindrical portion was first carved out of the brain above the ARC to minimise compression by the chronic lens. This method fulfils many requirements in neural imaging yet there are still some drawbacks. Aberrations in the GRIN lenses mean that cell resolution imaging is often restricted to the central portion of the lens, hence making the impact on the mouse larger than it need be. Furthermore, since images are transmitted from a head-mounted camera, light access to the brain for stimulation or other imaging techniques is impeded.

4.3 Single-Mode Optical Fibres

When measuring fluorescence or reflected intensity, a single-mode fibre (SMF) can only transfer one image pixel value at a time, yet it is not uncommon for an imaging technique to use such a concept. Scanning confocal microscopy, for example, does exactly that as each point at the object is scanned individually. Additionally, the small core sizes of single-mode fibres makes them effective pin holes and they have been used for fibre-based confocal microscopy. This has been shown by scanning the SMF relative to the optical axis itself [48] and by deflecting the SMF output beam by means of piezoelectric deflectors [49]. The drawback to these methods is the requirement for scanning equipment, leading to bulky assemblies at the object end of the fibre.

An alternative method for SMF endoscopy is to encode the spatial information spectrally, thereby increasing the bandwidth. In this method, broadband light coupled into an SMF at the proximal end is expanded and focussed onto a grating etched at the distal end. The light is diffracted by the grating and forms a line of illumination at the ob-

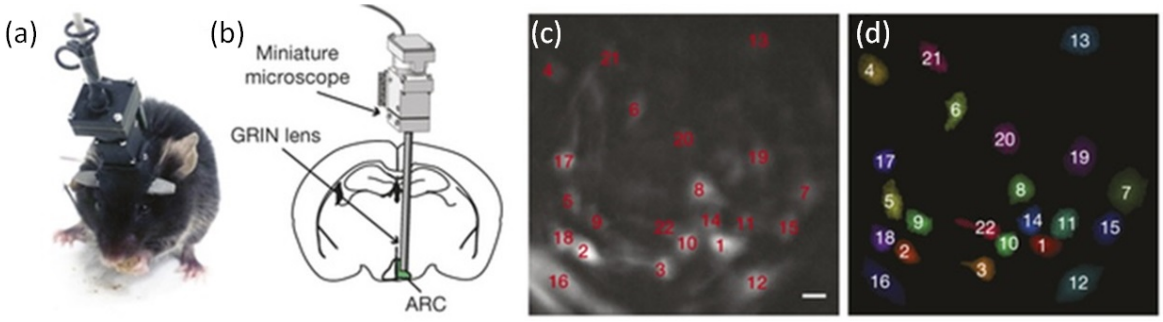

Figure 4: Commercially available head mounted microscope; (a) mouse with mounted microscope, (b) penetration depth to the ARC, (c) GCaMP fluorescence in neurons. Scale bar, 15 µm, (d) computationally segmented cells. Reprinted by permission from Macmillan Publishers Ltd: Nature [44], copyright (2015).

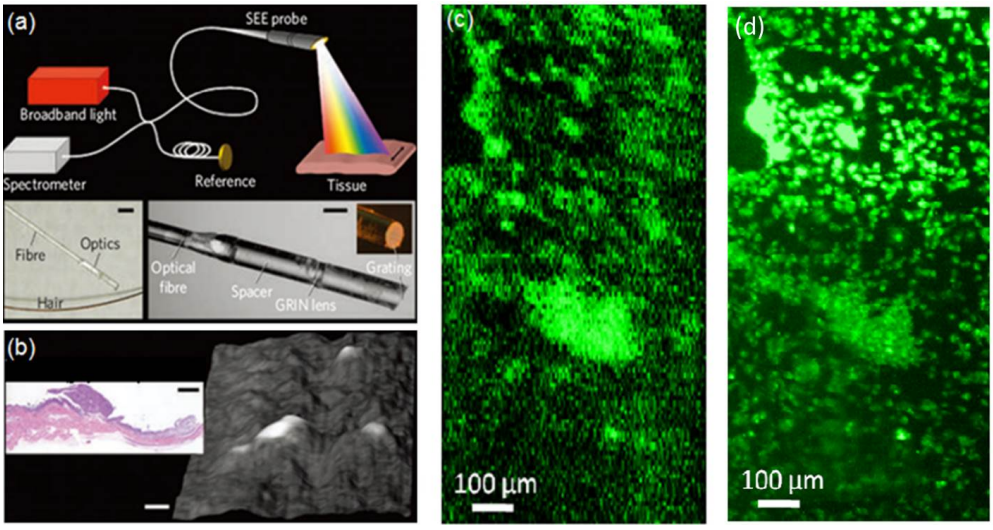

Figure 5: The principal behind, and examples of, spectrally encoded endoscopy (SEE). (a) Endoscope set up, comparison to a human hair (scale bar, 1 mm), and image of distal tip (scale bar, 0.5 mm), (b) Mouse ovarian tumour nodules overlaid on depth profile (scale bars, 0.35 mm), (c) SEE image of cultured epithelial cells labelled with green fluorescent dye, (d) Epifluorescent image of (c). (a) and (b) reprinted by permission from Macmillan Publishers Ltd: Nature [45], copyright (2006). (c) and (d) reprinted by permission from the Optical Society of America: Optics Express [46], copyright(2010).

ject. Since diffraction angles are wavelength-dependent, the spatial information of the object is encoded in the illumination spectrum. Reflected light is gathered and measured in a spectrometer. To scan the line across the sample the fibre is rotated. This technique has been used alongside a Michelson interferometer in order to extract depth information from a sample in a similar way to optical coherence tomography (OCT) [45]. It has also been demonstrated to work with a random scattering medium in place of a diffraction grating - thereby eliminating the need for scanning [50] - and in fluorescent microscopy [46].

In the case of fluorescence imaging, the resolution was somewhat poor as the number of points which can be resolved in a line is directly proportional to the bandwidth being imaged. In the reflection case, the illumination bandwidth was 250 nm, whereas green fluorescent protein (GFP) emission has a typical FWHM of ∼56 nm [51]. Figure 5 summarises spectrally encoded endoscopy (SEE). Fluorescent SEE has been reported to have a low collection efficiency which, when coupled to the low intensity emission of labelled cells, caused the method to become slow requiring dwell times of up to 500 ms per line [46]. Furthermore, the number of resolvable points on a single line in this method depends on the diameter of the collecting aperture, which is restricted in fibre endoscopy. Spectral encoding itself, however, could be used for fast high resolution imaging in the reflection regime as demonstrated by Goda *et al.* where micrometre resolution was imaged at an astounding frame rate of 6.1 MHz [52]. Their method is yet to be realised in fibres or fluorescent microscopy.

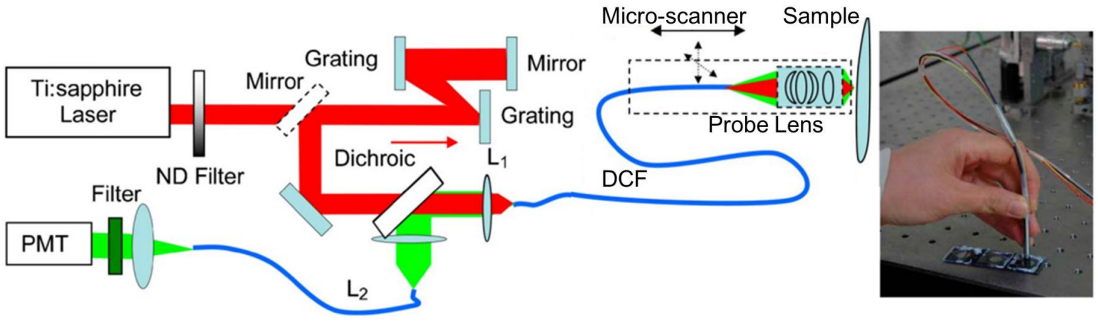

Figure 6: Piezoelectric scanning two-photon endoscope schematic, left, and device, right. Adapted by permission from the Optical Society of America: Optics Letters [47], copyright(2008).

4.4 Double-Clad Fibres

Double-clad fibres (DCF) are advantageous in imaging as they can offer both a narrow single-mode excitation beam through the inner core and a high NA collection objective through the outer core. They are used in much the same way as the single-mode fibres. Both fibres can be used in spectral encoding [53], and with microelectromechanical systems (MEMS) for scanning excitation [47].

Figure 6 shows a schematic of a two-photon flexible endoscope. The laser pulse is negatively chirped to compensate for chromatic dispersion in the core of a DCF. The excitation beam is scanned in a spiral pattern by a piezoelectric deflector and fluorescence is captured in the outer core. This method is reported to image a field of view of 475 µm × 475 µm at more than 20 Hz. Since it is a two-photon excitation process, it offers optical sectioning and the resolution is high enough for sub-cellular imaging. It has also been shown that such an endoscope can be used in trapping and particle manipulation [54]. Two-photon endoscopes have also been developed in hollow core photonic crystal fibres [55]. Since the excitation beam travels through air in the core, dispersion effects are minimal and no prechirping is required. This allows for a user-selected excitation wavelength without the need to change the set-up. The drawback of these methods is that the focussing and scanning optics at the end of the fibre make it too large for *in-vivo* experiments in sensitive areas such as the brain.

4.5 Fibre Bundles

Traditional flexible endoscopes make use of fibre bundles where each core in the bundle acts as an independent pixel. The main criticism of fibre bundles is their limited spatial resolution, which is dictated by the inter-core spacing. The inter-core spacing is in turn limited by the need to minimise cross talk. The benefit of the bundles, however, exists in their ability to be used independently of scanning optics allowing for fast image acquisition. To remedy the low resolution of the fibre, Ozbay *et al.* [56] described a setup in which a non-implanted electrowetting lens, used for selecting the imaging plane, was used in conjunction with an implanted 1 mm diameter GRIN lens at the distal tip of the fibre. This served to demagnify the core spacing and provided a sub-cellular resolution. To correct for aberrations, the proximal end of the fibre was imaged with a confocal microscope. A similar technique employed a micro-mirror array instead of a pinhole which allowed wide field, structured illumination, and single and multi-point confocal microscopy [57]. In addition to this, a separate laser, for ChR2 activation, illuminated a liquid crystal spatial light modulator (SLM) used to generate phase masks in a plane conjugate to the Fourier plane of the fibre input. This allowed for the generation of arbitrary intensity patterns on the input face which can then be delivered through the fibre to the targeted neurons. The method was implemented with a micro-objective too large for implantation. The fibre system was, therefore, head mounted and imaging depths were shallow.

A common method for axially resolved images in fibre bundles is structured illumination microscopy (SIM). SIM does not require scanning of many points, giving it an edge over confocal microscopy in terms of speed. It also allows for the rejection of out-of-focus light by illuminating with a series of spatially modulated patterns, leading to uniform illumination when out of focus. The in-focus portion of the fluorescence can then be determined from the modulated signal, whereas the unmodulated fluorescence can be rejected [58]. SIM is low in phototoxicity compared to scanning methods, as the light is distributed over the image plane [59]. Ford *et al.* [60] and Bozinovic *et al.* [61] both describe the use of this method in fibre bundles. These require further image processing when compared to conventional SIM, as the quasi-honeycomb structures of

the core play a role in limiting the resolution and modulating both the excitation pattern and the collected image, see Figure 7(e). Both of the processing methods ultimately obtain a lateral resolution of 2.6 μm, near the Nyquist limit of the fibre as dictated by the cores and the micro-objective used.

Light sheet microscopy is another method demonstrated in a fibre bundle setup by Engelbrecht *et al.* [62]. A custom-made, cylindrical GRIN lens (cGRIN) is coupled to an SMF transmitting the excitation beam. The beam is reflected at the tip of the cGRIN by a prism, so that the excitation plane is perpendicular to its axis. Fluorescence is captured by a second GRIN lens running parallel to the cGRIN. This is summarised in Figure 7. Light sheet microscopy is fast, optically-sectioned, and among the lowest in terms of phototoxicity, yet this setup, though miniaturised, remains large for *in-vivo* research. Engelbrecht *et al.* reported the need to cut a small wedge out of the brain for imaging.

The smallest, commercially-available bundles are in fact only 160 μm in diameter with ∼1600 cores. However, large distal optics are often necessary for both selecting an imaging plane away from the tissue damaging tip, and to enhance resolution by demagnifying the inter-core spacing. Methods have been demonstrated for lensless holographic imaging through fibre bundles which would also encode depth information of the tissue [63]. This does, however, require some fibre tip modification to provide a reference beam for holography. It also does not address the low resolution problem. Other lensless methods in fibre bundles stem from imaging techniques which use speckle correlation to reconstruct an object [64]. This hinges on the fact that an autocorrelation of a random speckle pattern is a sharply peaked function, thereby allowing the object autocorrelation to be well approximated by that of the image [65]. This was recently extended to near diffraction-limited resolution in lensless bundle endoscopy and could prove a valuable technique since it is also bend insensitive [64].

4.6 Multimode Fibres

A multimode fibre (MMF) has the capacity to couple light to several orthogonal modes making it suitable for fast parallel communication. The bandwidth of such a fibre could be up to two orders of magnitude greater than a bundle of comparable size [68]. Studies of propagation of light through scattering media have paved the way for the use of MMFs in imaging. In a scattering medium, a focussed spot is distorted spatially in amplitude and phase. At imaging intensities the distortion is, however, considered to be a linear process and can be reversed. An SLM can be used to apply an arbitrary phase and amplitude modulation to an input beam and, hence, provide the necessary light field to recover a diffraction-limited focus behind a scattering medium [69, 70]. For imaging, the acquisition of a complex-valued transmission matrix is needed. This maps each of the orthogonal input modes to each output mode behind the scattering medium [71]. Once the transmission matrix is known for a set of input and output modes an image can be reconstructed [72]. An MMF could be treated much like a scattering medium. An arbitrary light field impinging on the proximal end could be expressed as a superposition of fibre eigenmodes. These modes travel through the fibre with different propagation constants, giving a speckle pattern at the distal end that differs greatly from the field at the proximal face [73].

The imaging performed by Choi *et al.*, outlined in Figure 8, uses a speckle basis to measure the transmission matrix and reconstruct images [66]. Although this is convenient, it relies on the measurement of a complex valued speckle pattern at the proximal end of the fibre. For incoherent samples with a broad emission, the speckle pattern is suppressed [74]. This is the case for fluorescence emission. One solution was to use a bucket sensor to collect all fluorescence for each given speckle intensity pattern [75]. This method does not have a defined focal plane and is, therefore, demonstrated only for thin samples. With the use of an SLM, however, a series of phase masks could be chosen for imaging such that the focal point at the distal end of the fibre is scanned over the object [76–79]. Resolution was improved in this scanned-point method by correlating the reflected light field from a given point at the object with the SLM mask required to generate that point [67, 80]. This is, in essence, confocal microscopy, but so far has only been demonstrated in the reflection regime, see Figure 9. Further resolution enhancements saw the use of modified fibre tips for an increased NA [81].

One key difficulty with these methods is the acquisition speed. If we consider our example problem, an image rate of 10 Hz is required for calcium transients; however, low refresh rates of SLMs (20-100 Hz) mean that images could require as long as four minutes in acquisition time [67]. To overcome this Čižmár *et al.* reported the use of an SLM to generate many phase masks distributed spatially in the Fourier plane of the SLM. The masks were then scanned through with a fast acousto-optic deflector (AOD) [82, 83], see Figure 10. They reported 5.4 Hz imaging of a 36 × 36 pixel image with an SLM [82]. Computational methods exploiting the sparsity and quasi-sparsity in the image spectrum have been used in reconstruction of under sampled images where time constraints limited extra recordings [84]. This was done both for suppression

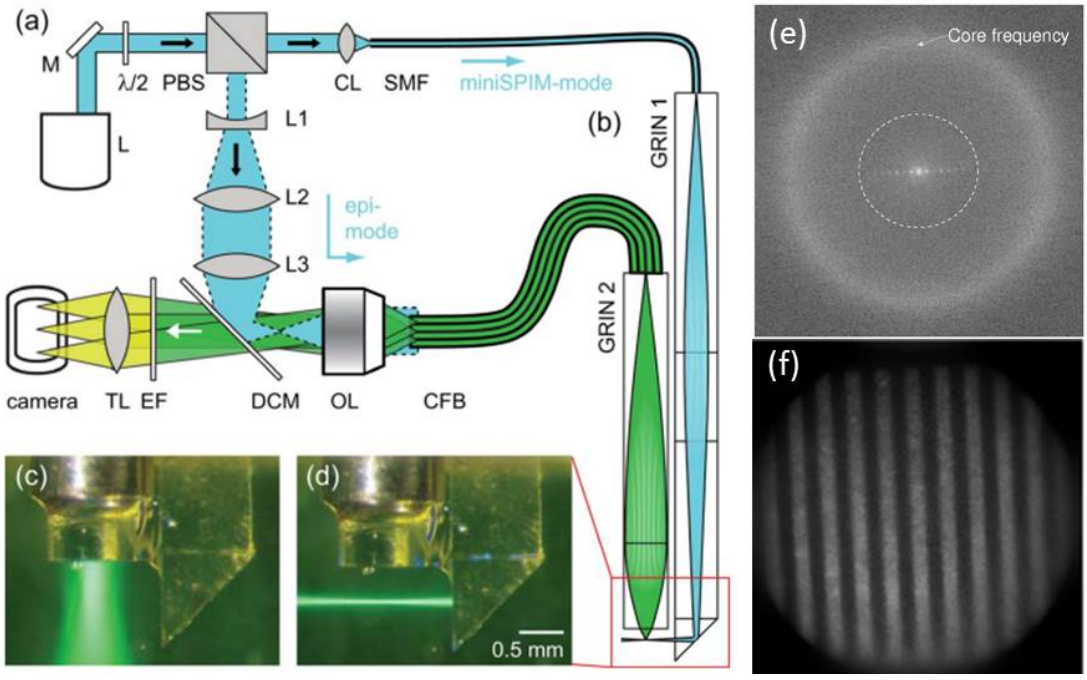

Figure 7: Fibre bundle light sheet microscopy (a) and (b) illustration of light sheet endomicroscope, (c) epifluorescent illumination (d) light sheet illumination, (e) Fourier transform of (f) imaged through fibre bundle; the diffuse ring corresponds to the core spatial frequencies. The Nyquist limit is half the radius shown by the dotted white line. (a)-(d) reprinted by permission from the Optical Society of America: Optics Letters [62], copyright(2010). (e) and (f) reprinted by permission from the Optical Society of America: Optics Express [61], copyright(2008).

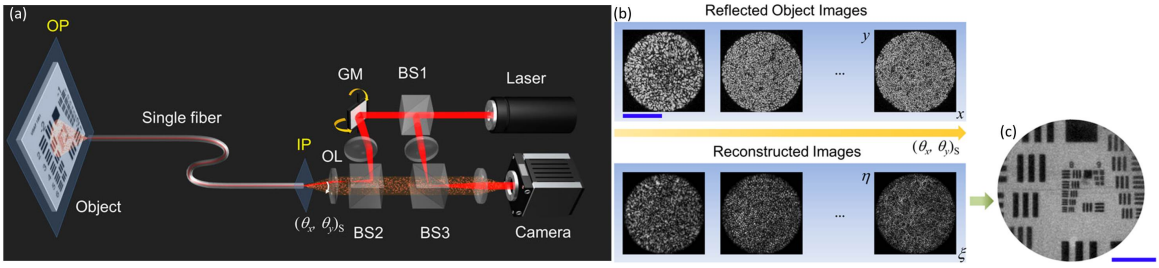

Figure 8: Example of speckle basis fibre imaging; (a) setup for imaging, (b) recorded and reconstructed speckle patterns (scale bar, 100 µm), (c) Sum of reconstructed images (scale bar, 50 µm). Reprinted by permission from the American Physical Society: Physical Review Letters [66], copyright(2012).

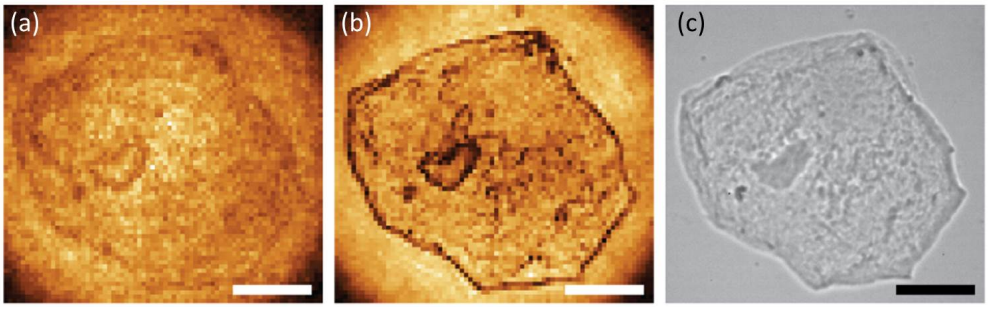

Figure 9: Human epithelial cell imaged with (a) fibre total intensity method, (b) fibre wavefront correlations, (c) transmission wide field control image. Scale bars, 20 µm. Reprinted by permission from the Optical Society of America: Optics Express [67], copyright(2015).

of noise [85] and in cases where extra measurements were not physically possible [86]. Enhancement of temporal resolution is also demonstrated with the use of digital micromirror devices (DMDs), which have refresh rates on the order of 20 kHz. DMDs, although only offering binary amplitude modulation, were shown to be effective at focussing and imaging through scattering media [87, 88]. DMDs have also been used in pixelation-free imaging through fibre bundles[89].

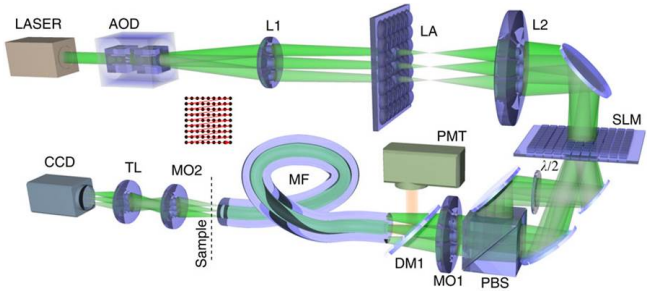

Figure 10: Fluorescence imaging set up with microlens array (LA) and acousto-optic deflector (AOD) for increased acquisition speed. Reprinted by permission from Macmillan Publishers Ltd: Nature Communications [82], copyright (2012).

Further advancements in MMF microscopy followed common techniques used in out-of-fibre setups. Plöschner *et al.* described a method by which the use of Bessel beams at the fibre output could be used in light sheet microscopy [90]. Although this is yet to be realised in a fibre-only endoscope, it has a great advantage in imaging live cells as light sheet methods have very low phototoxicity [19]. Steps towards two-photon imaging have also been made despite considerable challenges, as not only does the light suffer from modal dispersion, it has also been shown that, for broadband sources, the transmission matrix is wavelength dependent [91]. The modal dispersion can be compensated for with an SLM in graded index fibres over long distances by minimising power in higher order modes [92]. Morales-Delgado *et al.* [93] demonstrated spatial and temporal focussing of a 500 fs pulse of light through a step index fibre recently. They did so by selecting mode groups with similar phase velocities, thereby minimising modal dispersion. The modes within these groups were then modulated by the SLM to produce the spatially-focussed spot shown in Figure 11. Carpenter *et al.* observed Eisenbud-Wigner-Smith states in graded index fibres [94]. These states are the eigenstates of the delay operator of the fibre and, as such, exhibit the same temporal profile at the input and output. Since the eigenstates form an orthogonal basis it has been suggested that they could be used in imaging [95]. Further modifications to two-photon fibre-scopes involved undertaking phase conjugation through a fibre bundle [96]. Each core in the bundle carries a few modes and these could be later separated with a coherence gating. Using only the fundamental modes in each core effectively suppressed modal dispersion.

One of the biggest setbacks of using a multimode fibre probe for *in-vivo* imaging is the sensitivity to bending. Changes in the fibre shape quickly lead to mode scrambling and the focus point is lost [82, 97, 98]. Plöschner *et al.* formed a theoretical transmission matrix for short segments of step index fibre with corrections for dopant diffusion and refractive index changes due to internal stresses arising from bending the fibre [97]. They were able to calculate a theoretical deformation operator (DO) which described how the transmission matrix would change under a given small deformation. This implies that, in future applications of multimode endoscopy, the change in shape could be corrected for if it can be accurately monitored. The DO is applicable over the whole fibre face so that arbitrary holograms projected with the DO correction will be displayed accurately at the fibre output. This is in contrast to the method presented by Caravaca-Aguirre *et al.* [98] who used a field programmable gate array (FPGA) feedback mechanism to optimise a DMD mask for a single point intensity. The FPGA means this is done very quickly in the span of 37 ms, yet the method suffers two drawbacks: (i) it requires feedback from a distal end photodiode and (ii) it only corrects for a single point at the output. The use of a partially reflective coating on the distal end of the fibre has been suggested for dynamic updating of the fibre transmission matrix [99]. A similar method was employed by Farahi *et al.* who used a holographic guide star to determine the fibre conformation and a database of SLM masks for correction [100]. Recently, however, it has been demonstrated that phase conjugation in fibre bundles exhibits some bend insensitivity [101]. A bend in the fibre causes a phase difference between the cores and, hence, moves the focal point at the distal end. For small to moderate bends, the focus is not destroyed as mode mixing within each fibre core is minimal, giving this technique some promise. The methods incorporating MMFs in this section easily fulfill the size and spatial resolution constraints of our problem but struggle when it comes to flexibility and temporal resolution. Although efforts have been made in overcoming limitations of MMF endoscopes there are still more avenues to be explored.

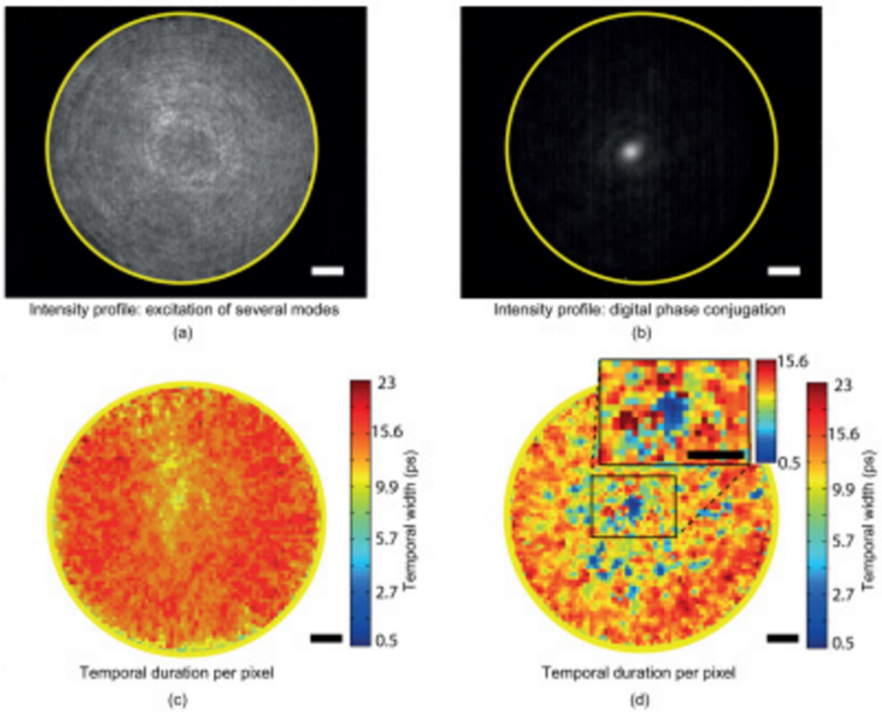

Figure 11: Multimode fibre output analysis of light pulse; (a) and (c) excitation of a large number of modes, (b) and (d) with digital phase conjugation. (a) and (b) show spatial profile of pulse intensity. (c) and (d) show pulse temporal width at each pixel. Reprinted by permission from the Optical Society of America: Optics Express [93], copyright(2015).

5 Conclusion

We have given a brief overview of many existing and emerging technologies which enable deep brain imaging and neuronal measurement. The example problem posed presents considerably challenging obstacles pertinent to this field of research. Since striatal research is very sensitive to cortical damage our attention was largely directed at lensless fibre techniques. These methods can offer very thin probes while maintaining a large transmission bandwidth. Yet, in spite of their advantages, they have their short comings: multimode fibre methods suffer inflexibility while fibre bundles offer low resolution or often end up requiring distal optics. No single solution fulfils all criteria and the expected success of these methods is largely dependent on what the user is willing to sacrifice. We therefore hope, through this problem, to motivate further development of minimally invasive probes and encourage the reader to use this review as a starting point to investigate more into this exciting topic.

Acknowledgement: This work was supported by the Okinawa Institute of Science and Technology Graduate University.

References

[1] J. Parkinson. *An Essay on the Shaking Palsy*. Sherwood, Neely and Jones, 1817.

[2] D. Ferrier. *The Functions of the Brain*. Smith, Elder and Co., 1876.

[3] A. F. Mettler. Effects of bilateral simultaneous subcortical lesions in the primate. *Journal of Neuropathology and Experimental Neurology*, 4(2):99–122, 1945.

[4] A. F. Mettler and C. C. Mettler. Effects of striatal injury. *Brain*, 65(3):242–255, 1942.

[5] A. V. Kravitz and A. C. Kreitzer. Striatal mechanisms underlying movement. *Physiology*, 27:167–177, 2012.

[6] C. R. Gerfen and D. J. Surmeier. Modulation of striatal projection systems by dopamine. *Annual Review of Neuroscience*, 34:441–466, 2011.

[7] G. Ji, M. E. Feldman, K. Deng, K. S. Greene, J. Wilson, J. C. Lee, R. C. Johnston, M. Rishniw, Y. Tallini, J. Zhang, W. G. Wier, M. P. Blaustein, H. Xin, J. Nakai, and M. I. Kotlikoff. Ca^{2+}-sensing transgenic mice postsynaptic signalling in smooth muscle. *Journal of Biochemistry*, 279:21461–21468, 2004.

[8] E. S. Boyden, F. Zhang, E. Bamberg, G. Nagel, and K. Deisseroth. Millisecond-timescale, genetically targeted optical control of neural activity. *Nature Neuroscience*, 8:1263–1268, 2005.

[9] F. Helmchen and W. Denk. Deep tissue two-photon microscopy. *Nature Methods*, 2(12):932–940, 2005.

[10] I. A. Favre-Bulle, D. Preece, T. A. Nieminen, L. A. Heap, E. K. Scott, and H. Rubinsztein-Dunlop. Scattering of sculpted light

in intact brain tissue, with implications for optogenetics. *Scientific reports*, 5, 2015.

[11] V. Ntziachristos. Going deeper than microscopy: The optical imaging frontier in biology. *Nature Methods*, 7(8):603–614, 2010.

[12] S. Schott, J. Bertolotti, J. F. Léger, L. Bourdieu, and S. Gigan. Characterization of the angular memory effect of scattered light in biological tissues. *Optics Express*, 23:13505–13516, 2015.

[13] S. L. Jacques. Optical properties of biological tissues: A review. *Physics In Medicine and Biology*, 58(11):R37–R61, 2013.

[14] R. Pierrat, P. Ambichl, S. Gigan, A. Haber, R. Carminati, and S. Rotter. Invariance property of wave scattering through disordered media. *Proceedings of the National Academy of Sciences*, 111(50):17765–17770, 2014.

[15] J. C. Jung, A. D. Mehta, E. Askay, R. Stepnoski, and M. J. Schnitzer. In vivo mammalian brain imaging using one- and two-photon fluorescence microendoscopy. *Journal of Neurophysiology*, 92:3121–3133, 2004.

[16] W. Wallace, L. H. Schaefer, and J. R. Swedlow. A workingperson's guide to deconvolution in light microscopy. *BioTechniques*, 31:1076–1097, 2001.

[17] X. Deng and M. Gu. Penetration depth of single-, two-, and three-photon fluorescence microscopic imaging through human cortex structures: Monte carlo simulation. *Applied Optics*, 42(16):3321–3329, Jun 2003.

[18] J. Larsch, D. Ventimiglia, C. I. Bargmann, and D. R. Albrecht. High-throughput imaging of neuronal activity in caenorhabditis elegans. *Proceedings of the National Academy of Sciences*, 110(45):E4266–E4273, 2013.

[19] B. C. Chen, W. R. Legant, K. Wang, L. Shao, D. E. Milkie, M. W. Davidson, C. Janetopoulos, X. S. Wu, J. A. Hammer III, Z. Liu, B. P. English, Y. Mimori-Kiyosue, D. P. Romero, A. T. Ritter, J. Lippincott-Schwartz, L. Fritz-Laylin, R. D. Mullins, D. M. Mitchell, J. N. Bembenek, A. C. Reymann, R. Böhme, S. W. Grill, J. T. Wang, G. Seydoux, U. S. Tulu, D. P. Kiehart, and E. Betzig. Lattice light-sheet microscopy: Imaging molecules to embryos at high spatiotemporal resolution. *Science*, 346(6208):1257998, 2014.

[20] R. A. Hoebe, C. H. Van Oven, T. W. J. Gadella, P. B. Dhonukshe, C. J. F. Van Noorden, and E. M. M. Manders. Controlled light-exposure microscopy reduces photobleaching and phototoxicity in fluorescence live-cell imaging. *Nature Biotechnology*, 25:249–253, 2007.

[21] V. Magidson and A. Khodjakov. Circumventing photodamage in live-cell microscopy. *Methods in cell biology*, 114, 2013.

[22] M. B. Bouchard, V. Voleti, C. S. Mendes, C. Lacefield, W. B. Grueber, Richard S. R. S. Mann, Randy M. R. M. Bruno, and E. M. C. Hillman. Swept confocally-aligned planar excitation (scape) microscopy for high-speed volumetric imaging of behaving organisms. *Nature Photonics*, 9(2):113–119, 2015.

[23] V. Voleti, M. B. Bouchard, C. Lacefield, R. M. Bruno, and E. M. Hillman. Fast, volumetric imaging of in vivo brains with swept confocally aligned planar excitation (scape) microscopy. In *Optics in the Life Sciences*, page BrM2B.3. Optical Society of America, 2015.

[24] E. Chaigneau, A. J. Wright, S. P. Poland, J. M. Girkin, and R. A. Silver. Impact of wavefront distortion and scattering on 2-photon microscopy in mammalian brain tissue. *Optics Express*, 19(23):22755–22774, 2011.

[25] P. Theer, M. T. Hasan, and W. Denk. Two-photon imaging to a depth of 1000 µm in living brains by use of a ti:al2o3 regenerative amplifier. *Optics Letters*, 28(12):1022–1024, 2003.

[26] D. Kobat, N. G. Horton, and C. Xu. In vivo two-photon microscopy to 1.6-mm depth in mouse cortex. *Journal of Biomedical Optics*, 16(10):106014, 2011.

[27] N. G. Horton, K. Wang, D. Kobat, C. G. Clark, F. W. Wise, C. B. Schaffer, and C. Xu. In vivo three-photon microscopy of subcortical structures within an intact mouse brain. *Nature Photonics*, 7(3):205–209, 2013.

[28] C. J. Roome and B. Kuhn. Chronic cranial window with access port for repeated cellular manipulations, drug application, and electrophysiology. *Frontiers in Cellular Neuroscience*, 8:379, 2014.

[29] J. L. Chen, M. L. Andermann, T. Keck, N. L. Xu, and Y. Ziv. Imaging neuronal populations in behaving rodents: Paradigms for studying neural circuits underlying behavior in the mammalian cortex. *The Journal of Neuroscience*, 33(45):17631–17640, 2013.

[30] D. A. Dombeck, A. N. Khabbaz, F. Collman, T. L. Adelman, and D. W. Tank. Imaging large-scale neural activity with cellular resolution in awake, mobile mice. *Neuron*, 56(1):4–57, 2007.

[31] P. Moshayedi, G. Ng, J. C.F. Kwok, G. S.H. Yeo, C. E. Bryant, J. W. Fawcett, K. Franze, and J. Guck. The relationship between glial cell mechanosensitivity and foreign body reactions in the central nervous system. *Biomaterials*, 35(13):3919–3925, 2014.

[32] S. Ghanavati, L. X. Yu, J. P. Lerch, and J. G. Sled. A perfusion procedure for imaging of the mouse cerebral vasculature by X-ray micro-CT. *Journal of Neuroscience Methods*, 221:70–77, 2014.

[33] L. Yu, K. Ronayne, T. Johnson, T. Fuzesi, J. Dunn, J. Bains, and K. Murari. Single fiber optical systems for monitoring brain dynamics in deep structures. In *Optics in the Life Sciences*, page JT3A.49. Optical Society of America, 2015.

[34] G. Cui, S. B. Jun, X. Jin, M. D. Pham, S. S. Vogel, D. M. Lovinger, and R. M. Costa. Concurrent activation of striatal direct and indirect pathways during action initiation. *Nature*, 494(7436):238–242, 2013.

[35] A. V. Kravitz and A. C. Kreitzer. Optogenetic manipulation of neural circuitry in vivo. *Current Opinion in Neurpbiology*, 21(3):433–439, 2011.

[36] E. S. Calipari, R. C. Bagot, I. Purushothaman, T. J. Davidson, J. T. Yorgason, C. J. Peña, D. M. Walker, S. T. Pirpinias, K. G. Guise, C. Ramakrishnan, K. Deisseroth, and E. J. Nestler. In vivo imaging identifies temporal signature of d1 and d2 medium spiny neurons in cocaine reward. *Proceedings of the National Academy of Sciences*, 113(10):2726–2731, 2016.

[37] L. A. Gunaydin, L. Grosenick, J. C. Finkelstein, I. V. Kauvar, L. E. Fenno, A. Adhikari, S. Lammel, J. J. Mirzabekov, R. D. Airan, K. A. Zalocusky, K. M. Tye, Anikeeva P., R. C. Malenka, and K. Deisseroth. Natural neural projection dynamics underlying social behavior. *Cell*, 157(7):1535–1551, 2014.

[38] G. Cui, S. B. Jun, X. Jin, G. Luo, M. D. Pham, D. M. Lovinger, S. S. Vogel, and R. M. Costa. Deep brain optical measurements of cell type-specific neural activity in behaving mice. *Nature Protocols*, 9(6):1213–1228, 2014.

[39] D. Karadaglić, R. Juškaitis, and T. Wilson. Confocal endoscopy via structured illumination. *Scanning*, 24:301–304, 2002.

[40] J. C. Jung and M. J. Schnitzer. Multiphoton endoscopy. *Optics Letters*, 28(11):902–904, Jun 2003.

[41] K. König, A. Ehlers, I. Riemann, S. Schenkl, R. Bückle, and M. Kaatz. Clinical two-photon microendoscopy. *Microscopy Research and Technique*, 70:398–402, 2007.

[42] B. A. Wilt, L. D. Burns, E. T. W. Ho, K. K. Ghosh, E. A. Mukamel, and M. J. Schnitzer. Advances in light microscopy for neuroscience. *Annual review of neuroscience*, 32:435, 2009.

[43] F. Wang, H. S. S. Lai, L. Liu, P. Li, H. Yu, Z. Liu, Y. Wang, and W. J. Li. Super-resolution endoscopy for real-time wide-field imaging. *Optics Express*, 23(13):16803–16811, 2015.

[44] J. N. Betley, S. Xu, Z. F. Huang Cao, R. Gong, C. J. Magnus, Y. Yu, and S. M. Sternson. Neurons for hunger and thirst transmit a negative-valence teaching signal. *Nature*, 521:180–185, 2015.

[45] D. Yelin, I. Rizvi, W. M. White, J. T. Motz, T. Hasan, B. E. Bouma, and G. J. Tearney. Three-dimensional miniature endoscopy. *Nature*, 443(7113):765, 2006.

[46] A. Abramov, L. Minai, and D. Yelin. Multiple-channel spectrally encoded imaging. *Optics Express*, 18(14):14745–14751, 2010.

[47] H. Bao, J. Allen, R. Pattie, R. Vance, and M. Gu. Fast handheld two-photon fluorescence microendoscope with a 475 μm × 475 μm field of view for in vivo imaging. *Optics Letters*, 33(12):1333–1335, 2008.

[48] R. S. Pillai, D. Lorenser, and D. D. Sampson. Deep-tissue access with confocal fluorescence microendoscopy through hypodermic needles. *Optics Express*, 19(8):7213–7221, 2011.

[49] S. J. Miller, C. M. Lee, B. P. Joshi, A. Gaustad, E. J. Seibel, and T. D. Wang. Targeted detection of murine colonic dysplasia in vivo with flexible multispectral scanning fiber endoscopy. *Journal of Biomedical Optics*, 17(2):021103, 2012.

[50] S. M. Kolenderska, O. Katz, M. Fink, and S. Gigan. Scanning-free imaging through a single fiber by random spatio-spectral encoding. *Optics Letters*, 40(4):534–537, 2015.

[51] E. K. Bomati, G. Manning, and D. D. Deheyn. Amphioxus encodes the largest known family of green fluorescent proteins, which have diversified into distinct functional classes. *Evolutionary Biology*, 9(77), 2009.

[52] K. Goda, K. K. Tsia, and B. Jalali. Serial time-encoded amplified imaging for real-time observation of fast dynamic phenomena. *Nature*, 458(30):1145–1149, 2009.

[53] D. Yelin, B. E. Bouma, S. H. Yun, and G. J. Tearney. Double-clad fiber for endoscopy. *Optics Letters*, 29(20):2408–2410, 2004.

[54] M. Gu, H. Bao, X. Gan, N. Stokes, and J. Wu. Tweezing and manipulating micro- and nanoparticles by optical nonlinear endoscopy. *Light Science & Applications*, 3:e126, 2014.

[55] N. P. Ghimire, H. Bao, and M. Gu. Broadband excitation and collection in fiber-optic nonlinear endomicroscopy. *Applied Physics Letters*, 103(073703), 2013.

[56] B. N. Ozbay, J. T. Losacco, R. Cormack, R. Weir, V. M. Bright, J. T. Gopinath, D. Restrepo, and E. A. Gibson. Miniaturized fiber-coupled confocal fluorescence microscope with an electrowetting variable focus lens using no moving parts. *Optics Letters*, 40(11):2553–2556, 2015.

[57] V. Szabo, V. Ventalon, C.and De Sars, J. Bradley, and V. Emiliani. Spatially selective holographic photoactivation and functional fluorescence imaging in freely behaving mice with a fiberscope. *Optics Letters*, 84(6):1157–1169, 2014.

[58] D. Karadaglić and T. Wilson. Image formation in structured illumination wide-field fluorescence microscopy. *Micron*, 39(7):808–818, 2008.

[59] L. Schermelleh, R. Heintzmann, and H. Leonhardt. A guide to super-resolution fluorescence microscopy. *Journal of Cell Biology*, 190(2):165–175, 2010.

[60] T. N. Ford, D. Lim, and J. Mertz. Fast optically sectioned fluorescence hilo endomicroscopy. *Journal of Biomedical Optics*, 17(2):021105, 2012.

[61] N. Bozinovic, C. Ventalon, T. Ford, and J. Metz. Fluorescence endomicroscopy with structured illumination. *Optics Express*, 16(11):8016–8025, 2008.

[62] C. J. Engelbrecht, F. Voigt, and F. Helmchen. Miniaturized selective plane illumination microscopy for high-contrast in vivo fluorescence imaging. *Optics Letters*, 35(9):1413–1415, 2010.

[63] O. Coquoz, R. Conde, F. Taleblou, and C. Depeursinge. Performances of endoscopic holography with a multicore optical fiber. *Applied Optics*, 34(31):7186–7193, Nov 1995.

[64] A. Porat, E. R. Andresen, H. Rigneault, D. Oron, S. Gigan, and O. Katz. Widefield lensless imaging through a fiber bundle via speckle correlations. *Optics Express*, 24(15):16835–16855, 2016.

[65] O. Katz, P. Heidmann, M. Fink, and S. Gigan. Non-invasive single-shot imaging through scattering layers and around corners via speckle correlations. *Nature photonics*, 8(10):784–790, 2014.

[66] Y. Choi, C. Yoon, M. Kim, T. D. Yang, C. Fang-Yen, R. R. Dasari, K. J.n Lee, and W. Choi. Scanner-free and wide-field endoscopic imaging by using a single multimode optical fiber. *Physical Review Letters*, 109(20):203901, 2012.

[67] D. Loterie, S. Farahi, I. Papadopoulos, A. Goy, D. Psaltis, and C. Moser. Digital confocal microscopy through a multimode fiber. *Optics Express*, 23(18):23845–23858, Sep 2015.

[68] D. Gloge. Weakly guiding fibers. *Applied Optics*, 10(10):2252–2258, 1971.

[69] I. M. Vellekoop, A. Lagendijk, and A. P. Mosk. Exploiting disorder for perfect focusing. *Nature Photonics*, 4(5):320–322, 2010.

[70] T. Čižmár, M. Mazilu, and K. Dholakia. In situ wavefront correction and its application to micromanipulation. *Nature Photonics*, 4(6):388–394, 2010.

[71] S. M. Popoff, G. Lerosey, R. Carminati, M. Fink, A. C. Boccara, and S. Gigan. Measuring the transmission matrix in optics: An approach to the study and control of light propagation in disordered media. *Physical Review Letters*, 104(100601), 2010.

[72] Y. Choi, T. D. Yang, C. Fang-Yen, P. Kang, K. J. Lee, R. R. Dasari, M. S. Feld, and W. Choi. Overcoming the diffraction limit using multiple light scattering in a highly disordered medium. *Physical Review Letters*, 107:023902, 2011.

[73] A.W. Snyder and J. Love. *Optical Waveguide Theory*. Science paperbacks. Springer, 1983.

[74] B. Redding, A. Cerjan, X. Huang, M. L. Lee, A. D. Stone, M. A. Choma, and H. Cao. Low spatial coherence electrically pumped semiconductor laser for speckle-free full-field imaging. *Proceedings of the National Acadamy of Sciences*, 12(5):1304–1309, 2015.

[75] R. N. Mahalati, R. Yu Gu, and J. M. Kahn. Resolution limits for imaging through multi-mode fiber. *Optics Express*, 21(2):1656–1668, 2013.

[76] T. Čižmár and K. Dholakia. Shaping the light transmission through a multimode optical fibre: complex transformation analysis and applications in biophotonics. *Optics Express*, 19(20):18871–18884, 2011.

[77] I. N. Papadopoulos, S. Farahi, C. Moser, and D. Psaltis. High-resolution, lensless endoscope based on digital scan-

ning through a multimode fiber. *Biomedical Optics Express*, 4(2):260–270, 2013.

[78] Bianchi S. and Di Leonardo R. A multi-mode fiber probe for holographic micromanipulation and microscopy. *Lab on a Chip*, 12(3):635–639, 2012.

[79] R. N. Mahalati, D. Askarov, J. P. Wilde, and J. M. Kahn. Adaptive control of input field to achieve desired output intensity profile in multimode fiber with random mode coupling. *Optics Express*, 20(13):14321–14337, 2012.

[80] D. Loterie, S. A. Goorden, D. Psaltis, and C. Moser. Confocal microscopy through a multimode fiber using optical correlation. *Optics Letters*, 40(24):5754–5757, Dec 2015.

[81] S. Bianchi, V. P. Rajamanickam, L. Ferrara, E. Di Fabrizio, C. Liberale, and R. Di Leonardo. Focusing and imaging with increased numerical apertures through multimode fibers with micro-fabricated optics. *Optics Letters*, 38(23):4935–4938, 2013.

[82] T. Čižmár and K. Dholakia. Exploiting multimode waveguides for pure fibre-based imaging. *Nature Communications*, 1027(3), 2012.

[83] M. Plöschner, B. Straka, K. Dholakia, and T. Čižmár. GPU accelerated toolbox for real-time beam-shaping in multimode fibres. *Optics Express*, 22(3):2933–2947, 2014.

[84] H. Jang, C. Yoon, E. Chung, W. Choi, and H. Lee. Speckle suppression via sparse representation for wide-field imaging through turbid media. *Optics Express*, 22(13):16619–16628, Jun 2014.

[85] R. Y. Gu, R. N. Mahalati, and J. M. Kahn. Noise-reduction algorithms for optimization-based imaging through multi-mode fiber. *Optics Express*, 22(12):15118–15132, Jun 2014.

[86] H. Jang, C. Yoon, E. Chung, W. Choi, and H. Lee. Holistic random encoding for imaging through multimode fibers. *Optics Express*, 23(5):6705–6721, 2015.

[87] D. B. Conkey, A. M. Caravaca-Aguirre, and R. Piestun. High-speed scattering medium characterization with application to focusing light through turbid media. *Opt. Express*, 20(2):1733–1740, 2012.

[88] A. Drémeau, A. Liutkus, D. Martina, O. Katz, C. Schülke, F. Krzakala, S. Gigan, and L. Daudet. Reference-less measurement of the transmission matrix of a highly scattering material using a dmd and phase retrieval techniques. *Optics Express*, 23(9):11898–11911, 2015.

[89] D. Kim, J. Moon, M. Kim, T. D. Yang, J. Kim, E. Chung, and W. Choi. Toward a miniature endomicroscope: pixelation-free and diffraction-limited imaging through a fiber bundle. *Optics Letters*, 39(7):1921–1924, 2014.

[90] M. Plöschner, V. Kollárová, Z. Dostál, J. Nylk, T. Barton-Owen, D. E. K. Ferrier, R. Chmelík, K. Dholakia, and T. Čižmár. Multimode fibre: Light-sheet microscopy at the tip of a needle. *Scientific reports*, 5, 2015.

[91] D. Andreoli, G. Volpe, S. Popoff, O. Katz, S. Grésillon, and S. Gigan. Deterministic control of broadband light through a multiply scattering medium via the multispectral transmission matrix. *Scientific Reports*, 5(10347), 2015.

[92] R. A. Panicker, J. M. Kahn, and S. P. Boyd. Compensation of multimode fiber dispersion using adaptive optics via convex optimization. *Journal of Lightwave Technology*, 26(10):1295–1303, 2008.

[93] E. E. Morales-Delgado, S. Farahi, I. N. Papadopoulos, D. Psaltis, and C. Moser. Delivery of focused short pulses through a multimode fiber. *Optics Express*, 23(7):9109–9120, 2015.

[94] J. Carpenter, B. J. Eggleton, and J. Schröder. Observation of eisenbud-wigner-smith states as principal modes in multimode fibre. *Nature Photonics*, 9(11):751–757, 2015.

[95] J. A. Carpenter, B. J. Eggleton, and J. Schroeder. Maximally efficient imaging through multimode fiber. In *CLEO: 2014*, page STh1H.3. Optical Society of America, 2014.

[96] D. B. Conkey, N. Stasio, E. E. Morales-Delgado, M. Romito, C. Moser, and D. Psaltis. Lensless two-photon imaging through a multicore fiber with coherence-gated digital phase conjugation. *Journal of Biomedical Optics*, 21(4):045002–045002, 2016.

[97] M. Plöschner, T. Tyc, and T. Čižmár. Seeing through chaos in multimode fibers. *Nature Photonics*, 9(8):529–535, 2015.

[98] A. M. Caravaca-Aguirre, E. Niv, D. B. Conkey, and R. Piestun. Real-time resilient focusing through a bending multimode fiber. *Optics Express*, 21(10):12881–12887, 2013.

[99] R. Y. Gu, R. N. Mahalati, and J. M. Kahn. Design of flexible multimode fiber endoscope. *Optics express*, 23(21):26905–26918, 2015.

[100] S. Farahi, D. Ziegler, I. N. Papadopoulos, D. Psaltis, and C. Moser. Dynamic bending compensation while focusing through a multimode fiber. *Optics Express*, 21(19):22504–22514, 2013.

[101] N. Stasio, D. B. Conkey, C. Moser, and D. Psaltis. Light control in a multicore fiber using the memory effect. *Optics Express*, 23(23):30532–30544, Nov 2015.